Published in final edited form as:
Magn Reson Med. 2010 March ; 63(3): 736–744. doi:10.1002/mrm.22227.

Effect of Blood Flow on Double Inversion Recovery Vessel Wall MRI of the Peripheral Arteries: Quantitation with T2 Mapping and Comparison with Flow-Insensitive T2-Prepared Inversion Recovery Imaging

Ryan Brown, PhD, **Thanh D. Nguyen, PhD**, **Pascal Spincemaille, PhD**, **Matthew D. Cham, MD**, **Grace Choi**, **Priscilla A. Winchester, MD**, **Martin R. Prince, MD PhD**, and **Yi Wang, PhD**
Department of Radiology, Weill Medical College of Cornell University, 1300 York Avenue, New York, NY 10065

Abstract

Blood suppression in the lower extremities using flow-reliant methods such as double inversion recovery (DIR) may be problematic due to slow blood flow. T2 mapping using fast spin echo (FSE) acquisition was utilized to quantitate the effectiveness of DIR blood suppression in 13 subjects and showed that 25 ± 12% of perceived vessel wall pixels in the popliteal arteries contained artifactual blood signal. To overcome this problem, a flow-insensitive T2-prepared inversion recovery (T2IR) sequence was implemented and optimal timing parameters were calculated for FSE acquisition. Black blood vessel wall imaging of the popliteal and femoral arteries was performed using 2D T2IR-FSE in the same 13 subjects. Comparison with 2D DIR-FSE showed that T2IR-FSE reduced wall-mimicking blood artifacts that inflated DIR-FSE vessel wall area measurements in the popliteal artery.

Keywords

black blood; vessel wall imaging; T2 prepared inversion recovery; femoral-popliteal artery; flow artifact; vessel wall thickness

INTRODUCTION

Arterial wall thickening is regarded a surrogate marker of atherosclerosis and wall thickness has been used to predict the risk of future cardiovascular events (1,2). Ultrasound imaging can measure the intima-media thickness (3) while magnetic resonance imaging (MRI) has been utilized for assessment of vessel wall thickness with the added benefits of plaque characterization and higher spatial resolution (4). Both techniques have been employed in serial imaging studies to measure wall thickness changes in response to drug therapy (5,6).

Vessel wall MRI requires suppression of blood signal (“black blood” [BB]) to delineate the vessel wall from the lumen. BB imaging is commonly performed using double inversion recovery (DIR) preparation (7,8) or spatial saturation (SPSAT) of upstream blood (9,10) followed by data acquisition such as fast spin echo (FSE) readout. DIR and SPSAT blood suppression rely on the inflow of blood with nulled signal into the imaging volume. Their

Corresponding author: Ryan Brown, PhD, 660 First Avenue, Room 442, New York, NY 10016, Phone: 212-263-3396, ryan.brown@nyumc.org.

effectiveness is therefore a function of volume thickness, blood velocity and flow pattern. These techniques provide excellent blood suppression for 2D imaging of arteries with fast blood flow such as the aorta, but may be less effective for 3D volumetric imaging and in the presence of recirculating or slow blood flow such as that observed near the carotid bifurcation (11) and in the peripheral arteries. To overcome these challenges, several BB preparation techniques have been recently developed including motion-sensitizing magnetization preparation (MSPREP) and T2-prepared inversion recovery (T2IR). MSPREP employs large velocity-encoding gradients to dephase moving blood spins prior to imaging and has been demonstrated to perform well in the heart (12), the aorta (13), and the carotid artery (14). Originally developed to suppress background signal in peripheral MR angiography (15), T2IR preparation has been proposed as a flexible technique to enhance blood-myocardium contrast in myocardial viability imaging (16) and to provide flow-insensitive blood suppression for cardiac and carotid BB imaging (17).

Although vessel wall MRI has been applied extensively to the aorta and the carotid artery (6,11,18), its utility for peripheral artery imaging has been demonstrated in only a handful of studies (19–23). A unique challenge associated with arterial wall imaging in the lower extremities is slow-moving and retrograde blood flow (24,25), which can be problematic for DIR and SPSAT techniques. While this problem is well recognized, the quantitation of slow blood flow effects on DIR vessel wall imaging has not been addressed. The application of MSPREP to BB lower extremity imaging may also be problematic because the rather slow and laminar blood flow requires large gradient switching, potentially leading to low wall signal due to eddy current effects (26). Flow-insensitive T2IR can be an effective approach to peripheral wall imaging; however, a clear guideline regarding the optimal selection of T2IR timing parameters is still lacking.

This work has three objectives: first, to quantify the effect of blood flow on 2D DIR-FSE images of the femoral and popliteal vessel wall based on the large T2 disparity between vessel wall and blood; second, to optimize T2IR-FSE timing parameters and investigate the feasibility of 2D T2IR-FSE for vessel wall imaging in the human lower extremities at 1.5 T; and third, to compare the signal-to-noise ratio (SNR), wall-to-lumen contrast-to-noise ratio (CNR), and wall area measurements obtained with DIR-FSE and T2IR-FSE techniques.

METHODS

DIR-FSE Imaging

To investigate the impact of stagnant blood flow on DIR-FSE wall imaging, the FSE product sequence was modified to enable multi-echo acquisition of images with 10 different effective TEs, thus permitting wall T2 measurements. Here the effective TE of an image was defined as the time at which the first echo in the echo train associated with that image was acquired, ranging from 9.4 ms to 347.8 ms with a step of 37.6 ms (echo spacing [ESP] = 9.4 ms, 4 echoes per effective TE).

A total of 13 volunteers (8 male, 5 female, age mean ± standard deviation [SD] of 37 ± 14 years, age range of 24–61 years) were imaged on a 1.5 T commercial scanner (GE Signa HDx, maximum gradient amplitude 33 mT/m, slew rate 120 T/m/s; Excite 14M5 software version; GE Healthcare, Waukesha, WI). This study was approved by our local institutional review board and written informed consent was obtained from all subjects prior to imaging. Signal reception was provided by a single-channel circular surface coil (7.5 cm diameter). Vector electrocardiographic (ECG) gating was used for cardiac synchronization. In each subject, cross-sectional BB FSE images of the right popliteal artery (at the level of the inferior condyle) and the right common femoral artery (at the level of the femoral triangle) were obtained in randomized order.

For each artery, 2D fast gradient echo images were acquired for vessel localization, followed by a series of low-resolution 2D DIR-FSE scout images to determine the optimal TI for blood suppression. The initial TI estimate was calculated automatically by the pulse sequence given a TR of 2 R-R intervals. This estimate was varied with a step of 100 ms until the luminal signal was comparable to the background noise (the typical TI was 700–900 ms). High-resolution 2D DIR-FSE images of the femoral and popliteal vessel wall were then acquired using the optimized TI. The remaining imaging parameters were similar to those used in recent vessel wall MRI studies (1,21): FOV = 12 cm; acquisition matrix size = 256 × 256 (interpolated to 512 × 512); TR = 2 R-R; slice thickness = 4 mm; DIR reinversion thickness = 4 mm; number of signal averages (NEX) = 3; receiver bandwidth = ±31.25 kHz; total echo train length (ETL) = 40; centric view ordering. A spectrally selective prepulse was used to suppress the periadventitial lipid signal for improved wall contrast. Parallel imaging was not used. The scan time was approximately 6.5 minutes for a nominal heart rate of 60 bpm.

Quantitation of DIR blood suppression

Arterial wall contours were determined from the initial echo image (which has the highest SNR). The well-defined lumen-wall boundary was determined automatically using a k-means clustering algorithm in ImageJ software (version 1.41; National Institutes of Health; Bethesda, MD). Due to limited contrast between the arterial wall and the surrounding tissues, the outer wall boundary was manually traced by an experienced radiologist using Advantage Workstation software (version 4.2; GE Healthcare, Waukesha, WI).

A semi-automated MATLAB (version 7.5; The Mathworks, Natick, MA) algorithm was used to classify the arterial wall pixels (identified using the previously obtained wall contours) as either “unaffected” or “partially affected” by blood signal. This algorithm is based on the premise that T2 of the media and adventitia vessel wall components measured in vivo at 1.5 T is approximately 50 ms or less (27). Correspondingly, the algorithm consisted of the following two steps:

Step 1 – Raw Segmentation—Because arterial wall T2 (approximately 50 ms for media and 25 ms for adventitia (27)) is much shorter than arterial blood T2 (approximately 290 ms (28)), an image acquired at an appropriately chosen TE can differentiate unaffected wall pixels (appearing relatively dark) from those with partial blood content (appearing relatively bright). The TE must be long enough to allow wall signal to decay to the noise floor (typically four times the wall T2), while keeping in mind that a shorter TE retains more blood signal. Consequently, the 7th echo image acquired at effective TE = 234 ms was selected as the cutoff in this study. The noise threshold was defined as the lumped mean plus three times the SD of pixel intensities measured from a user-selected region of background air free of image artifacts. Wall pixels with intensity below this threshold were deemed “unaffected” by blood, while those with intensity above were considered “partially affected.”

Step 2 – Refinement—For all wall pixels classified as “unaffected” after the first step, T2 was determined by fitting the signal intensities acquired at ten different effective TEs to a mono-exponential decay model $S = A + B*\exp(-TE/T2)$, where S is measured signal intensity, A denotes the signal offset, and B is the peak signal intensity. Lumped T2 mean and SD were calculated for this group of pixels. Of these pixels, only those with T2 less than the mean plus three times the SD were ultimately classified as “unaffected” while the rest were deemed outliers and reclassified as “partially affected.” This step prevented pixels with long T2 and low intensity from being incorrectly classified as vessel wall.

To further quantify blood and wall species within each pixel, DIR-FSE signal intensities at ten effective TEs were fit to a bi-exponential decay model $S = A + B*[f*\exp(-TE/T2_{wall}) + (1-f)*\exp(-TE/T2_{blood})]$, where f is the DIR-FSE partial wall content per pixel, $T2_{wall}$ was obtained from Step 2 above and $T2_{blood}$ was assumed to be 290ms. The corrected DIR-FSE wall area was defined as the product of the original DIR-FSE wall area and the mean partial wall content.

Optimization of BB T2IR-FSE Sequence for Vessel Wall Imaging

T2IR magnetization preparation integrates two classic preparation techniques—T2 preparation (29) for enhancing T2 contrast and inversion recovery (30) for enhancing T1 contrast—to provide increased flexibility in contrast manipulation between tissues with similar T1 but different T2 such as arterial blood and arterial vessel wall (Fig.1). For BB FSE imaging of the vessel wall, the T2IR timing parameters T2PREP and TI are chosen to null the blood signal while maximizing wall signal at the beginning of the FSE acquisition. Given T2PREP, the TI required to null the blood signal and the corresponding longitudinal magnetization of the wall can be calculated as follows (31,32):

$$\begin{aligned} TI &= T1_{blood}\ln[1+(1-\mathrm{Fexp}(-TD/T1_{blood}))\exp(-T2PREP/T2_{blood})] \\ &= T1_{blood}\ln[(1+\exp(-T2PREP/T2_{blood}))/(1+\mathrm{Fexp}(-(TR-TFSE)/T1_{blood})\exp(-T2PREP(1/T2_{blood}-1/T1_{blood})))]; \\ Mz_{wall}(TI) &\sim 1-\exp(-TI/T1_{wall})[1+(1-\mathrm{Fexp}(-TD/T1_{wall}))\exp(-T2PREP/T2_{wall})] \\ &\sim 1-\exp(-TI/T1_{wall})[1+\exp(-T2PREP/T2_{wall})]+\mathrm{Fexp}(-(TR-TFSE)/T1_{wall})\exp(-T2PREP(1/T2_{wall}-1/T1_{wall})) \end{aligned} \quad [1]$$

where TFSE = ETL*ESP is the length of the FSE readout, TD is the time delay between the center of the last echo in the echo train of the FSE acquisition and the 90_x tip-down pulse of the following T2IR sequence (Fig.1) and F is a scaling factor (see Eq.4 in (32)). To determine the optimal T2IR timing parameters, $Mz_{wall}(TI)$ is maximized with respect to T2PREP and TI subject to the constraints $Mz_{blood}(TI) = 0$. Accordingly, numerical optimization was performed for a typical range of TR (0.6–3 sec) and TFSE (0–400 ms) using MATLAB. The following tissue relaxation times were assumed at 1.5 T: $T1_{blood}$ = 1441 ms (28), $T2_{blood}$ = 290 ms (28), $T1_{wall}$ = 908 ms (extrapolated using $T1_{wall}$ at 9.4 T = 1892 ms (33) and $T1 \propto B_0^{4/10}$ (34)), $T2_{wall}$ = 48 ms (27). Note that for these T1 values (on the order of 1000 ms) and typical echo spacing of FSE acquisition (on the order of 10 ms), the scaling factor F in Eq.[1] is practically unity and thus can be ignored. Polynomial fitting was used to obtain empirical expressions for the optimal T2PREP and TI as a function of TR. These expressions were then programmed into the T2IR-FSE pulse sequence to enable automatic calculation of subject-specific T2PREP and TI for human imaging. The theoretical wall SNR ratio between the optimized T2IR-FSE and DIR-FSE sequences was also calculated as the ratio of the respective wall magnetizations at the beginning of the FSE readout.

T2IR-FSE Imaging

T2IR-FSE femoral and popliteal images were acquired in all volunteers with slice locations matched to DIR-FSE locations. The initial estimates of TI and T2PREP were calculated automatically given TR = 2 R-R intervals. A series of low-resolution 2D T2IR-FSE scout images were used to determine the optimal TI and T2PREP for blood suppression. The estimated T2PREP was not changed (typically 130 ms) while TI was varied with a step of

50 ms until the luminal signal was comparable to the background noise (the typical TI was 350–450 ms). High-resolution T2IR-FSE images of the vessel wall were then acquired with remaining imaging parameters and acquisition time identical to that for the DIR-FSE acquisition.

DIR-FSE and T2IR-FSE comparison

Vessel wall area was measured on DIR-FSE and T2IR-FSE images by subtracting the lumen area (measured by k-means clustering) from the outer wall area (measured by manual outlining). Wall SNR and wall-to-lumen CNR were measured using region-of-interest (ROI) analysis. The SD of pixel intensities in a large ROI placed in the background air of the magnitude image ($SD_{Rayleigh}$) was used to calculate the noise SD as $SD_{Gaussian} = 0.655 \times SD_{Rayleigh}$ for a single-channel receiver (35).

Flow Measurement

2D phase contrast (PC) imaging was performed with the same FOV, matrix size, slice thickness, receiver bandwidth and orientation as listed above and the following imaging parameters: TR = 7 ms; TE = 3.5 ms; flip angle = 30°; NEX = 1; velocity encoding (venc) = 60 cm/s (popliteal), 75 cm/s (femoral); 20 reconstructed cardiac phases. Acquisition time was approximately 65 sec for a heart rate of 60 bpm. Standard processing of PC data was carried out using commercial flow quantification software (Flow; version 3.2; Medis Medical Imaging Systems, Leiden, The Netherlands) to obtain blood flow measurements.

Statistical Analysis

All values are expressed as mean ± SD. Two-tailed paired-sample t-tests were used to assess the difference in the relative wall area partially affected incomplete DIR blood suppression between the imaged arterial locations, as well as the differences in wall SNR, wall-to-lumen CNR and wall area measurements between DIR-FSE and T2IR-FSE at each arterial location. Bland-Altman analysis (36) was performed to analyze the agreement between lumen and wall area measurements obtained with DIR-FSE and T2IR-FSE. P values of less than 0.05 were considered statistically significant.

RESULTS

Imaging experiments were completed successfully in all thirteen subjects. Table 1 shows the average relative wall area affected by incomplete DIR blood suppression identified using the wall pixel classification algorithm. The proportion of affected wall pixels was inversely related to blood velocity, with 24.9% observed in the popliteal artery compared to 13.8% in the femoral artery ($P < 0.05$); peak blood velocity was 40.7 ± 9.8 cm/s in the femoral artery and 25.8 ± 6.0 cm/s in the popliteal artery ($P < 0.001$).

Figure 2a shows the numerically optimized T2IR-FSE timing parameters as a function of typical TR and TFSE at 1.5 T. As TR increases, the optimal T2PREP changes slowly, while the optimal TI increases approximately as a negative quadratic function. Compared to DIR-FSE, the optimized T2IR-FSE sequence is expected to provide approximately 2–4 times less wall SNR over a typical TR range of 1–2 sec and TFSE range of 0–400 ms (Fig.2b).

T2 values for unaffected wall pixels based on mono-exponential fitting from DIR-FSE images were 52.5 ± 10.4 ms in the femoral artery wall and 48.1 ± 5.7 ms in the popliteal artery wall. Figure 3 shows examples of excellent DIR-FSE and T2IR-FSE images of the femoral and popliteal artery walls, demonstrating good qualitative agreement between the two techniques.

In three subjects, prominent blood flow artifacts mimicking thickened wall were observed in DIR-FSE popliteal images, whereas T2IR-FSE images were artifact-free (Figs.4 and 5). Figure 4 illustrates a case where blood signal (T2 ~ 290 ms) in DIR-FSE popliteal images persists in the image acquired at long effective TE of 234 ms, while signals from vessel wall and surrounding muscles (T2 ~ 50 ms or less) have already decayed. Figure 5 shows an example of DIR-FSE and T2IR-FSE images of the femoral and popliteal artery wall from another volunteer, demonstrating the increased presence of blood signal in DIR-FSE popliteal images compared to femoral images. In the femoral artery, peak blood flow was 39.5 cm/s with 3.3 mL/heartbeat stroke volume. A coherent rim of wall pixels with partial blood content can be detected in the DIR-FSE image where 11.8% of wall pixels were affected by blood, indicating adequate blood suppression. Correspondingly, vessel wall area measurements obtained from DIR-FSE and T2IR-FSE images were within 3% agreement. Blood flow was reduced in the popliteal artery, where peak velocity was 23.0 cm/s and stroke volume was 0.9 mL/heartbeat. Note that 50.4% of the wall pixels were affected by blood in the DIR-FSE image, indicating poor blood suppression. The DIR-FSE wall area measurement was 21.2% greater than that by T2IR-FSE, which can be attributed to the wall-mimicking blood artifact (arrowhead in Fig.5). While this artifact was indistinguishable from the vessel wall in the DIR-FSE image acquired at TE = 9.4 ms (short compared to wall T2), the artifact was highlighted by the developed wall pixel classification algorithm using images acquired at longer TEs. The mono-exponential T2 map corresponding to unaffected pixels showed values within the expected range for vessel wall, while longer T2 values are seen in the map corresponding to pixels affected by blood signal. Finally, bi-exponential fitting showed reduced partial wall content in the artifactual region and close to unity partial wall content elsewhere.

In one femoral and one popliteal case, the k-means clustering algorithm failed to correctly segment the lumen. In these two cases, the lumen was manually traced in both DIR-FSE and T2IR-FSE images. Over all subjects (N=13), the lumen was larger in T2IR-FSE images compared to DIR-FSE images in both the femoral (61.5 ± 21.2 mm^2 for T2IR vs. 59.3 ± 20.1 mm^2 for DIR, $P = 0.01$) and popliteal (31.1 ± 9.8 mm^2 for T2IR vs. 28.6 ± 8.6 mm^2 for DIR, $P < 0.001$) arteries (Table 2), suggesting the presence of slow blood flow pixels in DIR images. In contrast, a negligible difference was observed in DIR-FSE and T2IR-FSE outer wall area in both femoral ($P = 0.15$) and popliteal ($P = 0.07$) arteries. DIR-FSE and T2IR-FSE were found to provide similar wall area measurements in the femoral artery ($P = 0.24$), while the difference in the popliteal artery was marginally significant ($P = 0.04$). DIR-FSE partial wall content was 0.97 ± 0.03 and 0.95 ± 0.03 in the femoral and popliteal arteries, respectively. After correction of DIR-FSE wall areas for partial wall content, both techniques provided similar vessel wall areas in both femoral ($P = 0.85$) and popliteal ($P = 0.40$) arteries. Figure 6 shows the Bland-Altman comparison of lumen and vessel wall areas obtained with DIR-FSE and T2IR-FSE. Note that T2IR-FSE provided improved blood suppression at the cost of 32% and 50% lower SNR in the femoral and popliteal artery wall, respectively (Table 3).

DISCUSSION

Our preliminary results obtained in volunteers with no sign of peripheral arterial disease (PAD) show that DIR blood suppression was adequate in the femoral artery but less effective in the popliteal artery. This may be attributed to reduced blood velocity and stroke volume typical of lower extremity vessels. Although a velocity of only 0.6cm/s is required for blood to exit a 4mm slice for DIR blood suppression with TI=650ms, blood may be stagnant near the lumen-wall boundary and may reverse direction during diastole, resulting in incomplete blood suppression.. In contrast to DIR suppression, which relies on blood exchange, T2IR-FSE provided flow-insensitive blood suppression. In both femoral and

popliteal arteries, T2IR-FSE derived lumen area measurements were typically greater than DIR-FSE derived area measurements, indicating that incomplete DIR blood suppression gives rise to partial blood signal that may be misinterpreted as vessel wall.

Typical DIR-FSE vessel wall imaging utilizes only the initial echo for diagnosis. However, the initial echo contains signal from both blood and vessel wall which are difficult to differentiate given their similar signal intensity. In this work, a multi-echo acquisition was implemented to characterize DIR blood suppression by exploiting the T2 disparity between vessel wall and blood. Images at long echo times can be used to identify blood artifacts and exclude these regions from vessel wall classification. Vessel wall and blood differentiation is particularly important in the lower extremities where stagnant blood is more pronounced compared to other vessels such as the aorta. In the popliteal artery, DIR blood suppression was markedly poor in 3 of 13 subjects where substantial wall-mimicking artifacts such as those in Figs. 4 and 5 were observed. In other subjects, artifacts were less conspicuous but still present; on average, 25% of DIR popliteal artery wall pixels were affected by slow blood flow. It should be noted that due to partial volume effects, this may not translate directly into increased wall area. Similarly, since high pixel intensity in DIR-FSE images with long TE was attributed to incomplete blood suppression, it would be reasonable to assume that T2 values near that of blood (290 ms) would have been observed; however T2 values longer than 200 ms were rarely seen. This suggests partial volume effects resulted from incomplete DIR blood suppression yielding pixels with a mixture of blood and wall, and intermediate T2 values near the lumen-wall boundary. These partial volume effects are evident in Fig. 4, where the longest T2 values typically occur at the perceived wall-lumen boundary while shorter T2 values are observed in the outer periphery. Partial volume effects are also demonstrated in Fig. 5 where a region containing high blood content is highlighted using bi-exponential fitting.

These findings indicate that sophisticated blood suppression techniques such as MSPREP (12–14) or T2IR-FSE may be better suited for vessel wall imaging in the lower extremities. MSPREP flow spoiling is becoming more widespread for vessel wall imaging due to its applicability to 2D multi-slice or 3D acquisitions. However, like DIR, MSPREP relies on blood movement for effective suppression. In this study, we chose to implement T2IR-FSE sequence due to its insensitivity to blood velocity. While we have shown 2D T2IR to be a viable option for lower extremity vessel wall imaging, it is hindered by a long acquisition time (6.5 mins per slice) making it unsuitable for clinical application where coverage on the order of 20–30 cm is preferred. Analogous to the DIR acquisition, the long 2D T2IR acquisition time arises from its substantial idle time and multiple signal averages needed to boost SNR to resolve the thin artery wall. In contrast to DIR, T2IR blood suppression does not rely on slice selective pulses and may be readily converted to 3D acquisition which offers a vast improvement in efficiency. Further SNR gain may be realized using long fast spin echo readout with variable flip angles (37,38) and a multi-channel receive coil at higher magnetic field strength. Preliminary work utilizing these advances has produced 3D T2IR-FSE BB images of a 28 cm segment of the right and left femoral-popliteal artery with 0.7 mm isotropic resolution in approximately 8 mins at 3T using a commercially available 8-channel cardiac coil (39). Given these promising results, we expect 3D T2IR imaging to be a clinically useful tool for screening lower extremity vessels in normal patients or those with PAD.

Contrast enhanced (CE) vessel wall imaging has shown promise to detect atherosclerotic plaque (40–42). T2IR blood suppression relies on knowledge of wall and blood T1 and T2 relaxation times, which change dynamically after contrast injection. Techniques such as quadruple inversion recovery that minimizes variation of the magnetization signal using multiple inversion pulses have been developed to provide T1-insensitive flow suppression

(43). An analogous approach may be the subject of future work to reduce the T1 sensitivity of T2IR.

One limitation of the DIR-FSE and T2IR-FSE vessel wall area comparison is that the DIR-FSE sequence provided higher SNR than T2IR-FSE, which may inherently yield reduced T2IR-FSE area measurements. However, the wall area disparity between the two methods was inversely related to blood velocity, suggesting that incomplete DIR blood suppression, rather than higher SNR, was effectively responsible for inflated DIR-FSE popliteal vessel wall area measurements. Additionally, improved spatial resolution may reveal more precise differences in wall area measurements (44), as the true image resolution here (0.47 mm × 0.47 mm) was similar to the intima-media wall thickness expected in the common femoral artery (0.74 mm) (3). Note that DIR blood suppression effectiveness is inversely related to both slice thickness and reinversion slab thickness. In these experiments, a slice thickness of 4 mm was selected as a compromise wherein wall SNR, wall blurring due to artery curvature, and slice thickness used in previous vessel wall MRI studies were considered. The reinversion slab thickness was chosen to be the same as the imaging slice thickness to minimize the effect of slow blood flow. In typical imaging applications where the reinversion slab thickness is often set to a value 2–3 times larger than the imaging slice thickness, greater DIR slow blood artifacts than those reported here can be anticipated.

This study has several limitations. First, patients with clinically suspected atherosclerotic disease were not included. As PAD patients often have reduced blood velocity due to occlusion (24), we expect DIR blood artifacts to be more pronounced than those reported here. Therefore, flow insensitive blood suppression techniques such as T2IR may be more essential for the BB vessel wall imaging in the patient population. A second limitation is the lack of a reference standard for vessel wall area measurement such as B-mode or intravascular ultrasound. Thirdly, T1 and T2 of carotid vessel wall were used due to the lack of information on lower extremity wall. Arterial wall in the lower extremities often has thicker adventitia layer with shorter T2 than that of media (4). The resulting shorter wall T2 is not likely to affect the image analysis presented in this study. Fourth, manually traced outer wall contours may introduce variability in vessel wall area measurements. While automatic k-means clustering worked well for delineation of the wall-lumen boundary, reduced contrast between the arterial wall and surrounding structures (for example skeletal muscle and vein) prevented reliable outer wall segmentation. More advanced segmentation algorithms could be implemented to improve tracing repeatability (45). Finally, the DIR-FSE classification algorithm operates under the assumption that pixels corresponding to vessel wall have negligible signal at TE_{eff} of 234 ms. This is a reasonable conjecture for healthy or diseased (for example calcified, lipid core, or fibrotic) vessel wall, as these components are thought to have T2 of less than 70 ms at 1.5 T in vivo (27). However, it is possible that fluid or other long T2 substance could exist outside the vessel wall and contribute to partial blood pixels reported here.

In conclusion, DIR blood suppression has been quantified using T2-based measurements that showed DIR blood suppression may be inadequate for vessel wall imaging in the lower extremities where slow flowing blood is prominent. This inadequate blood suppression may result wall-mimicking blood artifacts and inflate vessel wall area measurements. As an alternative, T2IR preparation provides flow insensitive blood suppression required for imaging in these territories. Optimal T2IR timing parameters were calculated for FSE acquisition at 1.5T and applied to 13 subjects. These preliminary data were free of blood-mimicking artifacts and hence T2IR should be considered a feasible method for black blood imaging of the lower extremity vessel wall.

REFERENCES

1. Malayeri AA, Natori S, Bahrami H, Bertoni AG, Kronmal R, Lima JA, Bluemke DA. Relation of aortic wall thickness and distensibility to cardiovascular risk factors (from the Multi-Ethnic Study of Atherosclerosis [MESA]). Am J Cardiol 2008;102(4):491–496. [PubMed: 18678312]
2. Amarenco P, Cohen A, Tzourio C, Bertrand B, Hommel M, Besson G, Chauvel C, Touboul PJ, Bousser MG. Atherosclerotic disease of the aortic arch and the risk of ischemic stroke. N Engl J Med 1994;331(22):1474–1479. [PubMed: 7969297]
3. Smilde TJ, van den Berkmortel FW, Boers GH, Wollersheim H, de Boo T, van Langen H, Stalenhoef AF. Carotid and femoral artery wall thickness and stiffness in patients at risk for cardiovascular disease, with special emphasis on hyperhomocysteinemia. Arterioscler Thromb Vasc Biol 1998;18(12):1958–1963. [PubMed: 9848890]
4. Demarco JK, Rutt BK, Clarke SE. Carotid plaque characterization by magnetic resonance imaging: review of the literature. Top Magn Reson Imaging 2001;12(3):205–217. [PubMed: 11432578]
5. Underhill HR, Yuan C, Zhao XQ, Kraiss LW, Parker DL, Saam T, Chu B, Takaya N, Liu F, Polissar NL, Neradilek B, Raichlen JS, Cain VA, Waterton JC, Hamar W, Hatsukami TS. Effect of rosuvastatin therapy on carotid plaque morphology and composition in moderately hypercholesterolemic patients: a high-resolution magnetic resonance imaging trial. Am Heart J 2008;155(3):584, e581–e588. [PubMed: 18294500]
6. Corti R, Fuster V, Fayad ZA, Worthley SG, Helft G, Smith D, Weinberger J, Wentzel J, Mizsei G, Mercuri M, Badimon JJ. Lipid lowering by simvastatin induces regression of human atherosclerotic lesions: two years' follow-up by high-resolution noninvasive magnetic resonance imaging. Circulation 2002;106(23):2884–2887. [PubMed: 12460866]
7. Edelman RR, Chien D, Kim D. Fast selective black blood MR imaging. Radiology 1991;181(3): 655–660. [PubMed: 1947077]
8. Yarnykh VL, Yuan C. Multislice double inversion-recovery black-blood imaging with simultaneous slice reinversion. J Magn Reson Imaging 2003;17(4):478–483. [PubMed: 12655588]
9. Felmlee JP, Ehman RL. Spatial presaturation: a method for suppressing flow artifacts and improving depiction of vascular anatomy in MR imaging. Radiology 1987;164(2):559–564. [PubMed: 3602402]
10. Nayak KS, Rivas PA, Pauly JM, Scott GC, Kerr AB, Hu BS, Nishimura DG. Real-time black-blood MRI using spatial presaturation. J Magn Reson Imaging 2001;13(5):807–812. [PubMed: 11329205]
11. Steinman DA, Rutt BK. On the nature and reduction of plaque-mimicking flow artifacts in black blood MRI of the carotid bifurcation. Magn Reson Med 1998;39(4):635–641. [PubMed: 9543426]
12. Nguyen TD, de Rochefort L, Spincemaille P, Cham MD, Weinsaft JW, Prince MR, Wang Y. Effective motion-sensitizing magnetization preparation for black blood magnetic resonance imaging of the heart. J Magn Reson Imaging 2008;28(5):1092–1100. [PubMed: 18972350]
13. Koktzoglou I, Li D. Diffusion-prepared segmented steady-state free precession: Application to 3D black-blood cardiovascular magnetic resonance of the thoracic aorta and carotid artery walls. J Cardiovasc Magn Reson 2007;9(1):33–42. [PubMed: 17178678]
14. Wang J, Yarnykh VL, Hatsukami T, Chu B, Balu N, Yuan C. Improved suppression of plaque-mimicking artifacts in black-blood carotid atherosclerosis imaging using a multislice motion-sensitized driven-equilibrium (MSDE) turbo spin-echo (TSE) sequence. Magn Reson Med 2007;58(5):973–981. [PubMed: 17969103]
15. Brittain JH, Olcott EW, Szuba A, Gold GE, Wright GA, Irarrazaval P, Nishimura DG. Three-dimensional flow-independent peripheral angiography. Magn Reson Med 1997;38(3):343–354. [PubMed: 9339435]
16. Liu CY, Wieben O, Brittain JH, Reeder SB. Improved delayed enhanced myocardial imaging with T2-Prep inversion recovery magnetization preparation. J Magn Reson Imaging 2008;28(5):1280–1286. [PubMed: 18972338]
17. Liu, C-Y.; Wieben, O.; Brittain, JH.; Reeder, SB. Proceedings of the 16th Annual Meeting of ISMRM. Toronto, Ontario, Canada: 2008. Flow-independent T2-prepared inversion recovery black blood MR imaging; p. 3079

18. Simonetti OP, Finn JP, White RD, Laub G, Henry DA. "Black blood" T2-weighted inversion-recovery MR imaging of the heart. Radiology 1996;199(1):49–57. [PubMed: 8633172]
19. Yang Q, Liu J, Barnes SR, Wu Z, Li K, Neelavalli J, Hu J, Haacke EM. Imaging the vessel wall in major peripheral arteries using susceptibility-weighted imaging. J Magn Reson Imaging 2009;30(2):357–365. [PubMed: 19629989]
20. Meissner OA, Rieger J, Rieber J, Klauss V, Siebert U, Tato F, Pfeifer KJ, Reiser M, Hoffmann U. High-resolution MR imaging of human atherosclerotic femoral arteries in vivo: validation with intravascular ultrasound. J Vasc Interv Radiol 2003;14(2 Pt 1):227–231. [PubMed: 12582191]
21. Isbell D, Meyer CH, Rogers WJ, Epstein FH, DiMaria JM, Harthun N, Wang H, Kramer CM. Reproducibility and reliability of atherosclerotic plaque volume measurements in peripheral arterial disease with cardiovasculr magnetic resonance. J Cardiovasc Magn Reson 2007;9:71–76. [PubMed: 17178683]
22. Coulden RA, Moss H, Graves MJ, Lomas DJ, Appleton DS, Weissberg PL. High resolution magnetic resonance imaging of atherosclerosis and the response to balloon angioplasty. Heart 2000;83(2):188–191. [PubMed: 10648495]
23. Wyttenbach R, Gallino A, Alerci M, Mahler F, Cozzi L, Di Valentino M, Badimon JJ, Fuster V, Corti R. Effects of percutaneous transluminal angioplasty and endovascular brachytherapy on vascular remodeling of human femoropopliteal artery by noninvasive magnetic resonance imaging. Circulation 2004;110(9):1156–1161. [PubMed: 15326071]
24. Mohajer K, Zhang H, Gurell D, Ersoy H, Ho B, Kent KC, Prince MR. Superficial femoral artery occlusive disease severity correlates with MR cine phase-contrast flow measurements. J Magn Reson Imaging 2006;23(3):355–360. [PubMed: 16463304]
25. Bogren HG, Buonocore MH. Blood flow measurements in the aorta and major arteries with MR velocity mapping. J Magn Reson Imaging 1994;4(2):119–130. [PubMed: 8180449]
26. Wang, J.; Yarnykh, VL.; Chu, B.; Yuan, C. Proceedings of the 16th Annual Meeting of ISMRM. Toronto, Ontario, Canada: 2008. Improved motion-sensitized driven equilibrium (iMSDE) blood-suppression sequence for atherosclerosis plaque imaging at 3T; p. 961
27. Toussaint JF, LaMuraglia GM, Southern JF, Fuster V, Kantor HL. Magnetic resonance images lipid, fibrous, calcified, hemorrhagic, and thrombotic components of human atherosclerosis in vivo. Circulation 1996;94(5):932–938. [PubMed: 8790028]
28. Stanisz GJ, Odrobina EE, Pun J, Escaravage M, Graham SJ, Bronskill MJ, Henkelman RM. T1, T2 relaxation and magnetization transfer in tissue at 3T. Magn Reson Med 2005;54(3):507–512. [PubMed: 16086319]
29. Brittain JH, Hu BS, Wright GA, Meyer CH, Macovski A, Nishimura DG. Coronary angiography with magnetization-prepared T2 contrast. Magn Reson Med 1995;33(5):689–696. [PubMed: 7596274]
30. Hajnal JV, Bryant DJ, Kasuboski L, Pattany PM, De Coene B, Lewis PD, Pennock JM, Oatridge A, Young IR, Bydder GM. Use of fluid attenuated inversion recovery (FLAIR) pulse sequences in MRI of the brain. Journal of computer assisted tomography 1992;16(6):841–844. [PubMed: 1430427]
31. Does MD. Relaxation-selective magnetization preparation based on T1 and T2. J Magn Reson 2005;172(2):306–311. [PubMed: 15649757]
32. Meara S, Barker G. Evolution of the longitudinal magnetization for pulse sequences using a fast spin-echo readout: application to fluid-attenuated inversion-recovery and double inversion-recovery sequences. Magn Reson Med 2005;54:241–245. [PubMed: 15968670]
33. Toussaint JF, Southern JF, Fuster V, Kantor HL. T2-weighted contrast for NMR characterization of human atherosclerosis. Arterioscler Thromb Vasc Biol 1995;15(10):1533–1542. [PubMed: 7583524]
34. McRobbie, DW.; Moore, EA.; Graves, MJ.; Prince, MR. MRI from picture to proton. Cambridge, UK: Cambridge University Press; 2003. p. 135-163.
35. Constantinides CD, Atalar E, McVeigh ER. Signal-to-noise measurements in magnitude images from NMR phased arrays. Magn Res Med 1997;38:852–857.
36. Bland J, Atman D. Measuring agreement in method comparison studies. Stat Methods Med Res 1999;8(2):135–160. [PubMed: 10501650]

37. Mugler, J.; H, M.; B, K. Proceedings of the 11th Annual Meeting ISMRM. Toronto, Ontario, Canada: 2003. Practical implementation of optimized tissue-specific prescribed signal evolutions for improved turbo-spin-echo imaging; p. 203

38. Hennig J, Weigel M, Scheffler K. Calculation of flip angles for echo trains with predefined amplitudes with the extended phase graph (EPG)-algorithm: principles and applications to hyperecho and TRAPS sequences. Magn Reson Med 2004;51(1):68–80. [PubMed: 14705047]

39. Nguyen, T.; Kawaji, K.; Spincemaille, P.; Cham, M.; Winchester, P.; Prince, M.; Wang, Y. Proceedings of the 21st Annual International Conference on Magnetic Resonance Angiography. East Lansing, Michigan, USA: 2009. 3D peripheral vessel wall MRI with flow-insensitive blood suppression and isotropic resolution at 3 tesla; p. 3.8

40. Zhao, X.; Cai, J.; Underhill, H.; Oikawa, M.; Dong, L.; Ota, H.; Hatsukami, T.; Yuan, C. Proceedings of the 17th Annual Meeting of ISMRM. Honolulu, Hawaii, USA: 2009. Minimization of MR contrast weightings for the comprehensive evaluation of carotid atherosclerotic disease; p. 602

41. Cai J, Hatsukami TS, Ferguson MS, Kerwin WS, Saam T, Chu B, Takaya N, Polissar NL, Yuan C. In vivo quantitative measurement of intact fibrous cap and lipid-rich necrotic core size in atherosclerotic carotid plaque: comparison of high-resolution, contrast-enhanced magnetic resonance imaging and histology. Circulation 2005;112(22):3437–3444. [PubMed: 16301346]

42. Takaya N, Cai J, Ferguson MS, Yarnykh VL, Chu B, Saam T, Polissar NL, Sherwood J, Cury RC, Anders RJ, Broschat KO, Hinton D, Furie KL, Hatsukami TS, Yuan C. Intra-and interreader reproducibility of magnetic resonance imaging for quantifying the lipid-rich necrotic core is improved with gadolinium contrast enhancement. J Magn Reson Imaging 2006;24(1):203–210. [PubMed: 16739123]

43. Yarnykh VL, Yuan C. T1-insensitive flow suppression using quadruple inversion-recovery. Magn Reson Med 2002;48(5):899–905. [PubMed: 12418006]

44. Mitsouras, D.; Mulkern, RV.; Owens, CD.; Cai, T.; Whitmore, AG.; Ersoy, H.; Conte, MS.; Creager, MA.; Rybicki, FJ. Proceedings of the 16th Annual Meeting of ISMRM. Toronto, Ontario, Canada: 2008. High-resolution T1- and T2-weighted black blood inner volume 3D fast spin echo imaging for characterizing vessel wall components in vivo; p. 958

45. Kerwin W, Xu D, Liu F, Saam T, Underhill H, Takaya N, Chu B, Hatsukami T, Yuan C. Magnetic resonance imaging of carotid atherosclerosis: plaque analysis. Top Magn Reson Imaging 2007;18(5):371–378. [PubMed: 18025991]

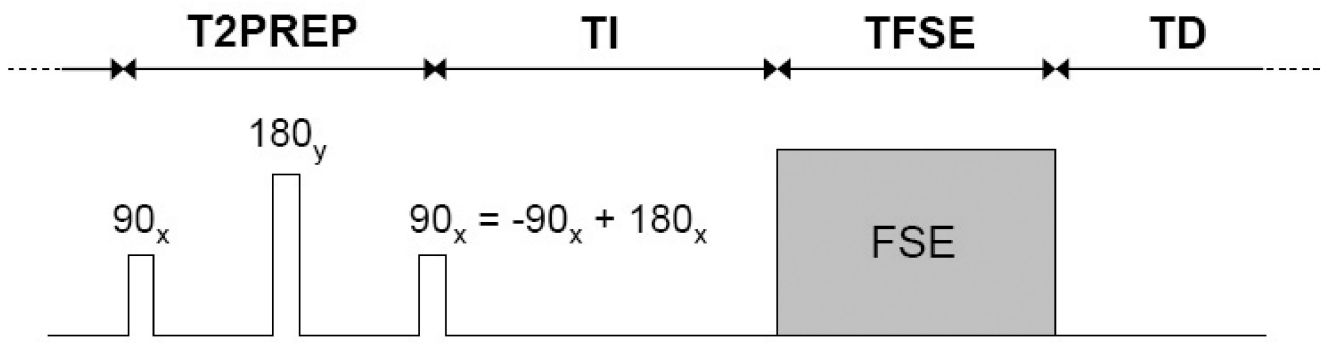

Figure 1.
Schematic of the implemented T2IR-FSE sequence for flow-insensitive BB imaging of the vessel wall. The T2IR magnetization preparation combines two commonly used contrast-enhancing techniques: T2 preparation (consisting of 90_x tip-down, 180_y refocusing, and -90_x tip-up RF pulses) for T2 contrast, and inversion recovery (consisting of a 180_x inversion pulse) for T1 contrast. Note that the -90_x tip-up of the T2 preparation and the 180_x inversion pulse can be conveniently combined into a single 90_x pulse as shown. Given repetition time TR = T2PREP + TI + TFSE + TD, the timing parameters (T2PREP, TI and TD) are chosen to null the blood signal while maximizing the wall signal at the beginning of the FSE acquisition (see text for details). Note that all RF pulses are spatially non-selective and correspondingly the T2IR technique can provide global suppression of blood regardless of its movement, a major advantage over the conventional DIR technique.

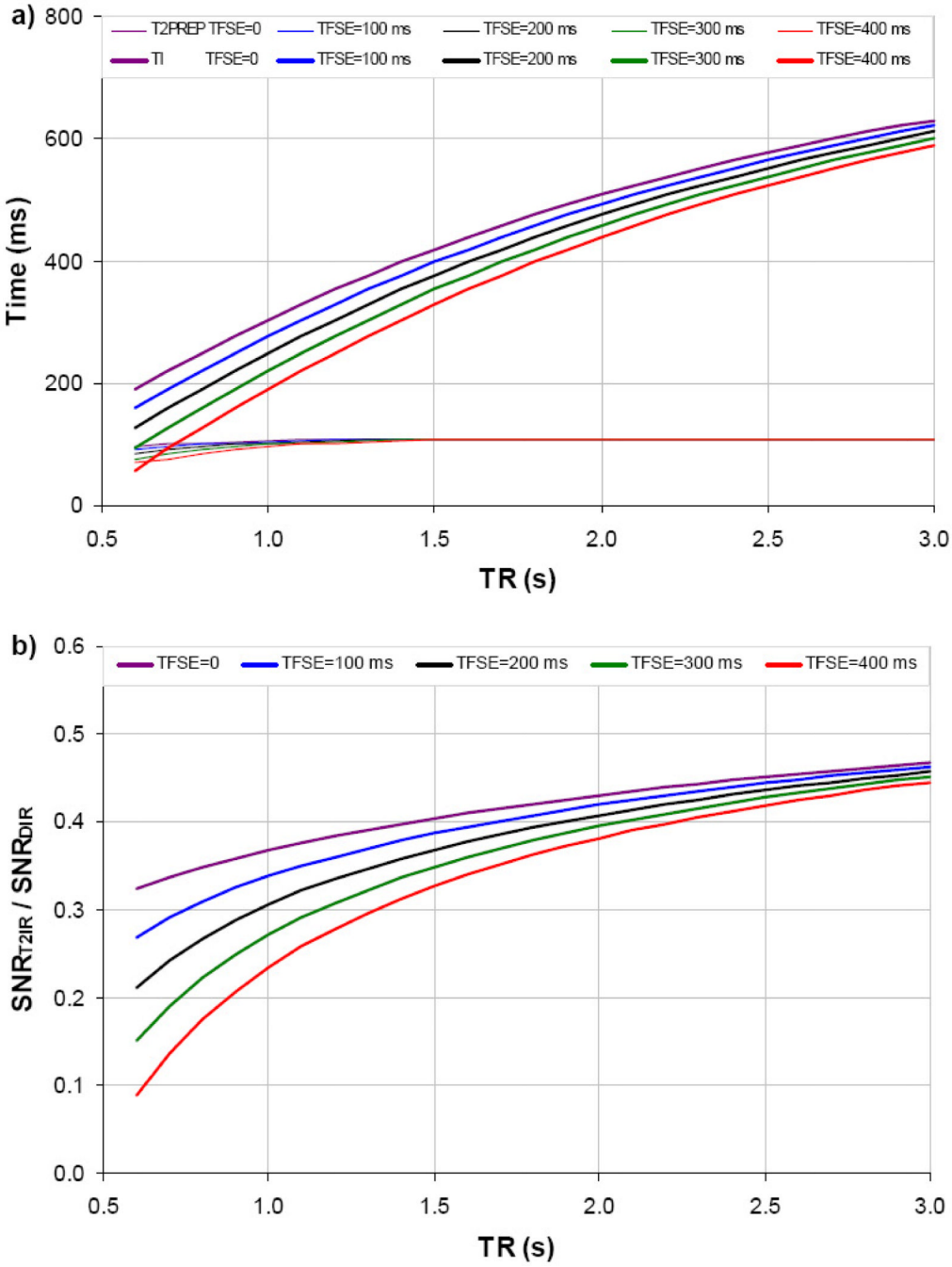

Figure 2.

Optimal T2PREP and TI as a function of TR and TFSE for BB T2IR-FSE vessel wall imaging at 1.5 T (a). Corresponding theoretical relative wall SNR between optimized T2IR-FSE and DIR-FSE is shown in b.

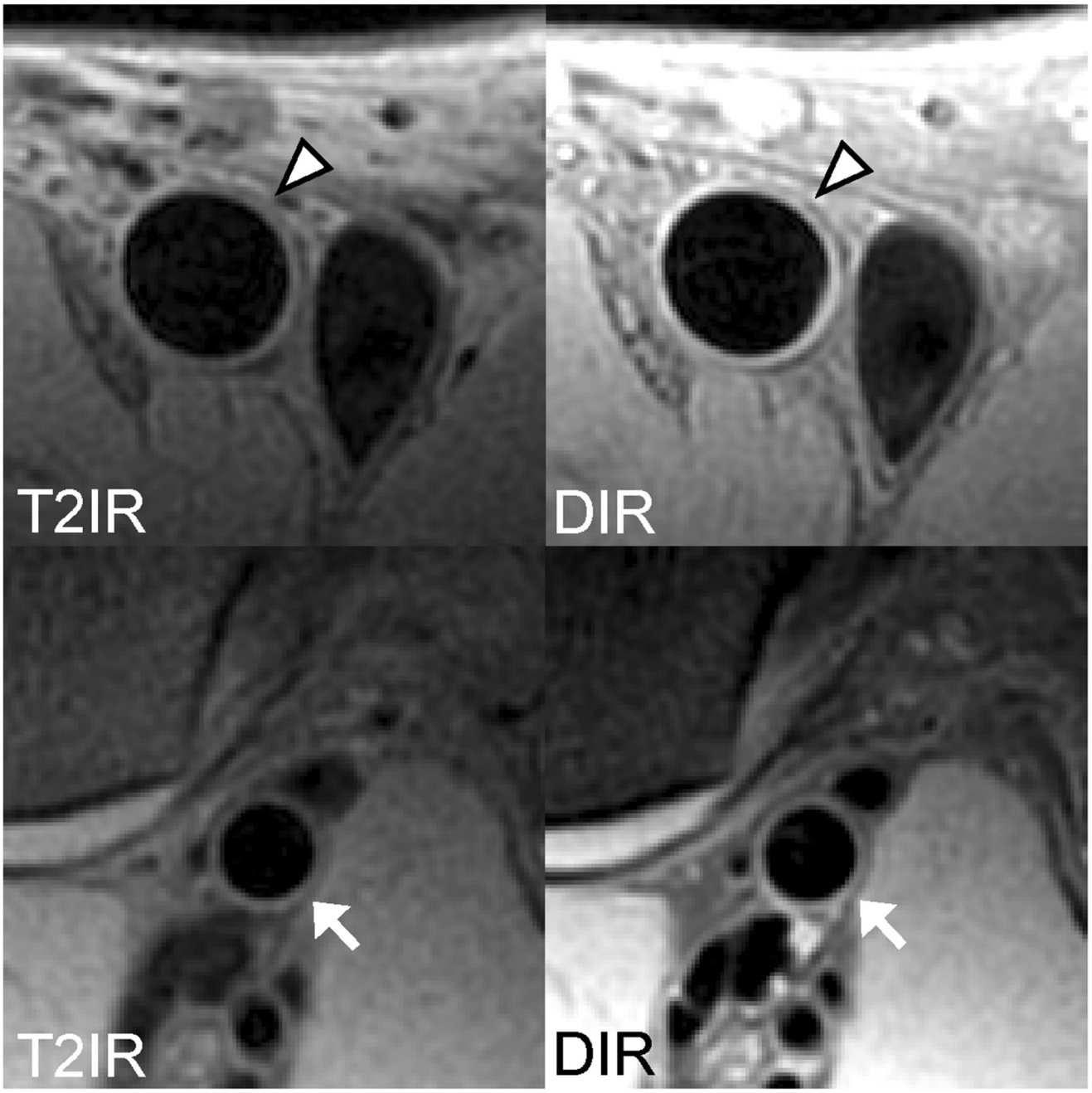

Figure 3.
Concordant femoral (arrowheads) and popliteal (arrows) vessel wall images obtained with T2IR-FSE and DIR-FSE. Note the effective arterial blood suppression by both techniques.

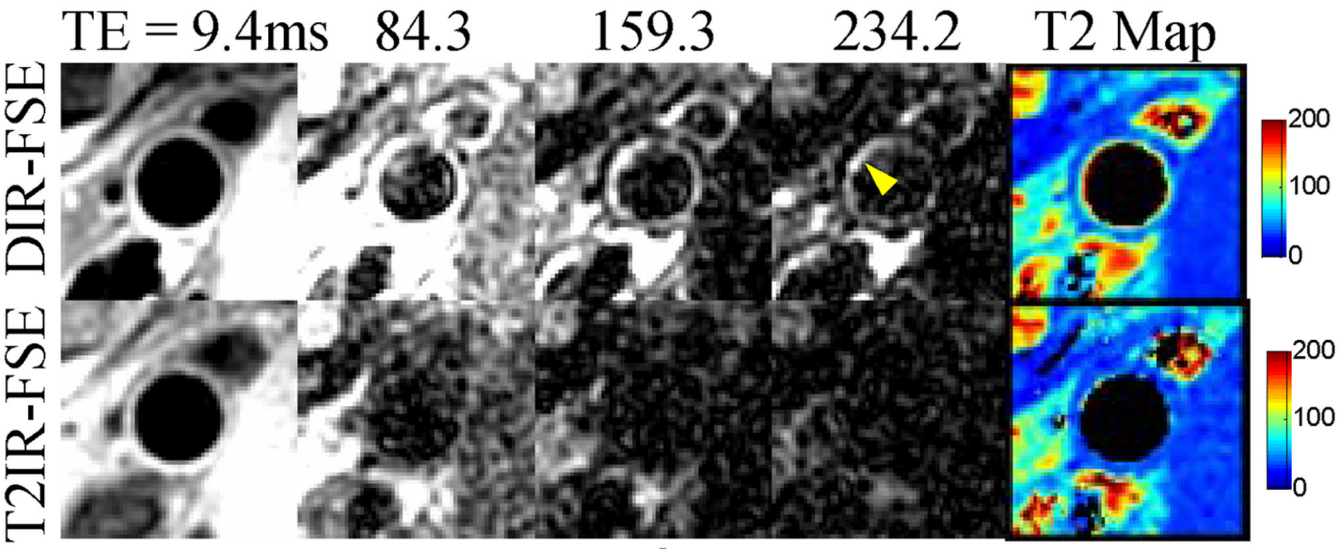

Figure 4.

Blood artifact (arrowhead) at the popliteal wall-lumen border in the DIR-FSE images (top row). While this artifact is not obvious with effective TE of 9.4 ms, it is conspicuous in images acquired at longer effective TEs where wall components and surrounding muscles with short T2s have decayed. The DIR-FSE T2 map shows elevated T2 values along the wall-lumen interface, indicating the presence of blood signal. These artifacts are absent in the T2IR-FSE images and corresponding T2 map (bottom row).

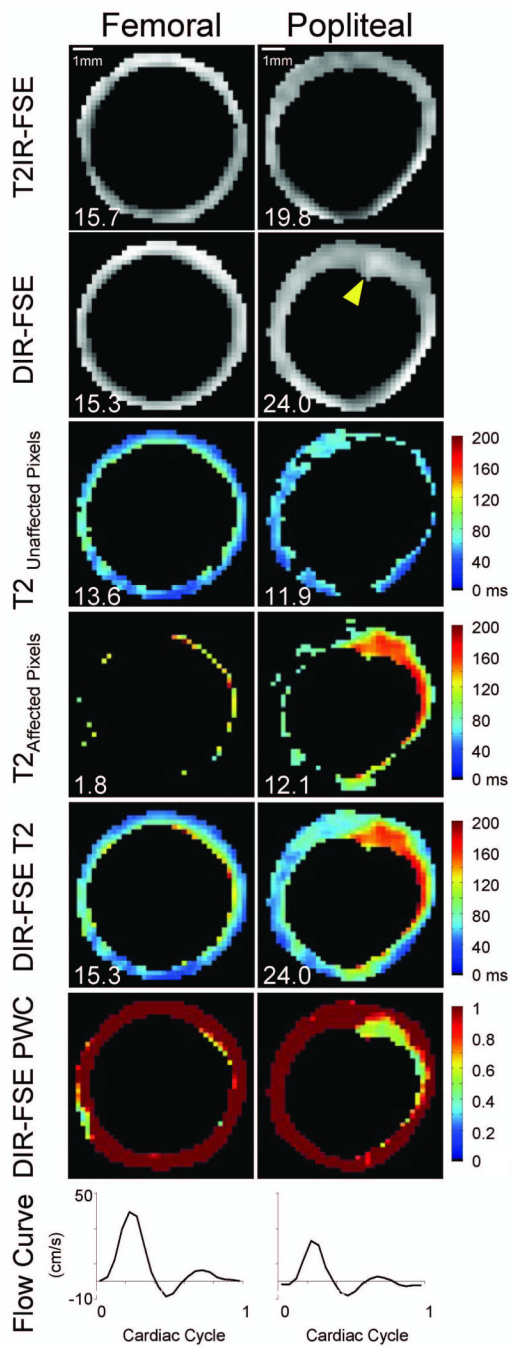

Figure 5.

Representative data set highlighting DIR-FSE popliteal blood artifact. Top row: segmented T2IR-FSE images at effective TE = 9.4 ms; second row: segmented DIR-FSE images at effective TE = 9.4 ms; third row: DIR-FSE T2 maps for unaffected vessel wall pixels; fourth row: DIR-FSE T2 maps for pixels affected by slow flowing blood; fifth row: collective DIR-FSE T2 maps; sixth row: DIR-FSE partial wall content (PWC) maps; and bottom row: blood velocity curves. The arrowhead in the DIR-FSE popliteal image indicates an area of incomplete blood suppression. The scale is indicated in the top row. Corresponding areas (in mm^2) are inset for reference.

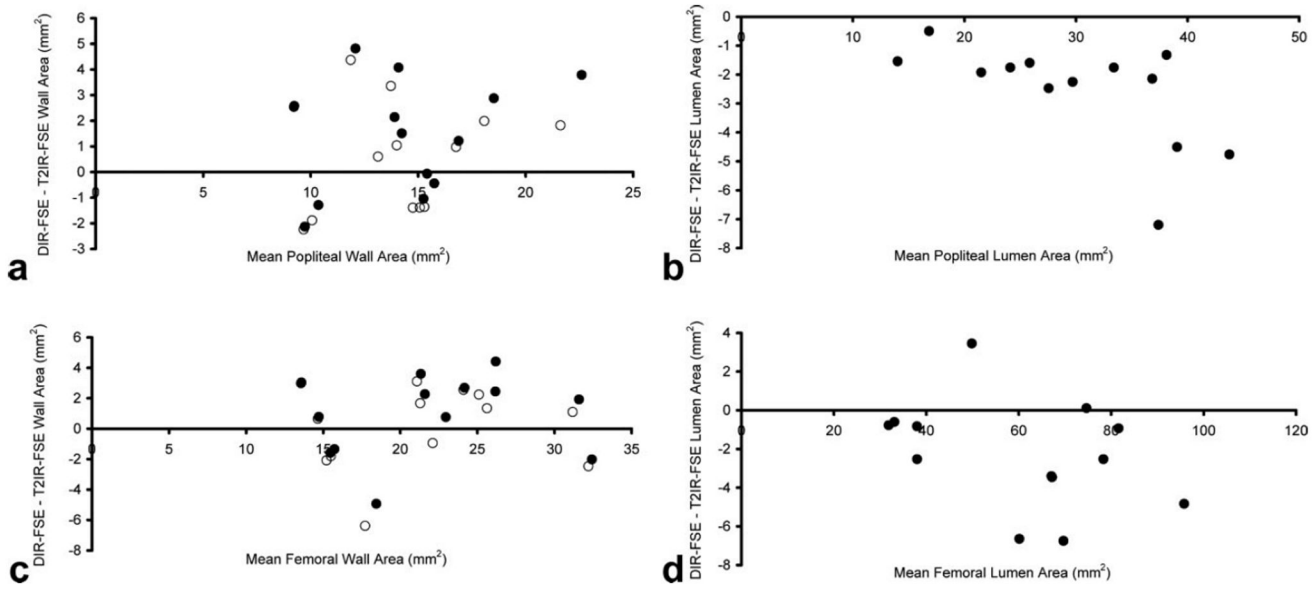

Figure 6.

Bland-Altman plots of wall area (a, b) and lumen area (c, d) measurements obtained with 2D DIR-FSE and T2IR-FSE imaging. Before DIR-FSE partial wall content correction (solid circles), agreement was 1.4 ± 2.2 mm^2 for the popliteal wall (a) and 0.9 ± 2.7 mm^2 for the femoral wall (b). After DIR-FSE partial wall content correction (open circles), agreement was 0.6 ± 2.1 mm^2 for the popliteal wall and 0.2 ± 2.8 mm^2 for the femoral wall. Popliteal lumen area bias was -2.6 ± 1.8 mm^2 (c) while femoral lumen area bias was -2.3 ± 2.8 mm^2 (d).

Table 1

Relative DIR-FSE wall area affected by incomplete blood suppression, blood velocity and stroke volume measured in the common femoral and popliteal arteries (N = 13).

	Ratio of affected and total wall pixels	Peak blood velocity (cm/s)	Stroke volume (mL/heartbeat)
Femoral artery	0.14 ± 0.10	40.7 ± 9.8	6.7 ± 4.3
Popliteal artery	0.25 ± 0.12	25.8 ± 6.0	1.4 ± 1.0
P	0.02	<0.001	<0.001

Table 2

Femoral and popliteal vessel wall and lumen area measurements obtained with 2D DIR-FSE and T2IR-FSE imaging (N = 13).

	Femoral artery			Popliteal artery		
	T2IR	**DIR**	**DIR corrected**	**T2IR**	**DIR**	**DIR corrected**
Wall (mm^2)	21.4 ± 6.1	22.3 ± 6.6	21.6 ± 6.4	13.8 ± 3.5	15.2 ± 4.2	14.4 ± 3.8
P		0.24	0.85		0.04	0.40
Lumen (mm^2)	61.5 ± 21.2	59.3 ± 20.1	N/A	31.1 ± 9.8	28.6 ± 8.6	N/A
P		0.01	N/A		<0.001	N/A

Magn Reson Med. Author manuscript; available in PMC 2010 August 13.

Table 3

SNR and CNR comparison of DIR-FSE and T2IR-FSE of femoral and popliteal artery wall (N = 13).

	SNR			CNR		
	T2IR	**DIR**	**P**	**T2IR**	**DIR**	**P**
Femoral artery	32 ± 16	47 ± 27	0.002	28 ± 15	42 ± 27	0.003
Popliteal artery	53 ± 15	107 ± 30	<0.0001	46 ± 16	93 ± 29	<0.0001